# Papers

*Volume 8: 2008-2014*

Thoft-Christensen, Palle

*Publication date:*
2014

*Document Version*
Publisher's PDF, also known as Version of record

# CHAPTER 147

# STOCHASTIC ANALYSIS OF THE INFLUENCE OF TOWER SHADOW ON FATIGUE LIFE OF WIND TURBINE BLADE[1]

R. Pedersen, S.R.K. Nielsen & P. Thoft-Christensen
Aalborg University, Aalborg, Denmark

## ABSTRACT

Fatigue damage accumulation in upwind turbine blades is primarily influenced by turbulence in the inflow. However, the stress reversals during blade passages through the stagnating and deflected mean wind field in front of the tower also contribute significantly. In the paper the lower order statistical moments of the fatigue life of a blade are estimated and compared for a turbine with a tripod tower and a standard mono-tower, respectively. The stagnation zones for each of the legs of the tripod are narrower than for the mono-tower, and hence the stress reversals will be comparable smaller. The blade stresses are calculated from a dynamic mechanical model based on a two dynamic degree of freedom. The self-induced aero-elastic loading and the turbulence loading are modeled by means of a quasi-static model linearized around the operational point, ignoring any memory effects on the load coefficients. However, such memory effects are taken into consideration at the calculation of the aero-dynamic load during tower passage by the use of a rational approximation to the relevant indicial function. Based on Monte Carlo simulations it is demonstrated that the expected damage accumulation per unit of time in the turbine blades are reduced significantly for the tripod when compared to the damage in a comparable mono-tower design.

[1] Structural Safety, Vol. 35, 2012, pp. 63-71

## 1. INTRODUCTION

Tower shadow is aero-dynamic disturbances of the wind flow due to the presence of the tower. The stress variation in the blades during tower passage depends on the size of the stagnation zone which is determined from the radius of the tower and the clearance of the blade from the tower(s). A decreased tower radius for the same clearance means a reduced stagnation zone and less stress variations. During tower passage the blades of a horizontal axis upwind wind turbine hit a zone of stagnating and deflected mean wind velocities. Due to the short time interval spent in the stagnation zone the tower shadow has ignorable influence on the power production. In any case the loads from tower shadow effect must be included in the design load case according to the IEC norm [1, Section 7.5].

Various aspects of the shadow effect has been extensively analyzed in the literature. Wang and Coton [2] considered tower shadow for down-wind turbines, where the shadow effect is even more pronounced. Dolan and Lehn [3] compared the oscillations of the rotor torque during tower passage and the oscillations due to the mean wind shear using a quasi-static model for the tangential coefficient. They showed that the oscillations are significantly influenced by the tower shadow effect. Munduate and Coton [4] made wind tunnel experiments with a two-bladed down-wind turbine, and concluded that the delay of non-stationary changes of the angle of attack has significant impact on the resultant normal coefficient, which determines the aero-dynamic load in the blade direction. This delay effect must be included in the formulation via a memory integral. Munduate and Coton [5] showed that the tower passage may trigger off dynamic stall, which in turn increases the dynamic response of the blade due to the loss of aero-dynamic damping. Wang [6] presents two strategies for computation of the aero-dynamic loadings associated with tower shadow on downwind. In one approach the velocity deficit is explicitly included in the wake model, whereas in the other model is based on a near wake model of the vorticity trailed from the blade. The physical model representing the shadow effect put forward by Rosas et al. [7] assumes that the tower reduces only the upstream horizontal free flow mean velocity. This reduction can be modeled with good accuracy by a potential flow field. The disturbance of the flow is in the interval of azimuth angle between [$-\pi/2$, $\pi/2$] because the flow above the tower height is assumed to be unaffected by the presence of the tower. Crawford [8] presents a tower shadow model that accounts for the retardation (or acceleration) of the flow due to the presence of the tower. The model smoothly blends a potential flow model upstream of the tower described by Moriarty and Hansen [9] and with a wake deficit model downstream used by Powles [10]. Fatigue damage accumulation in up-wind turbine blades is primarily caused by turbulence in the inflow. However, the stress reversals during blade passages through the tower shadow also contributes significantly.

The present paper analyses the possibility of reducing the expected damage accumulation during tower passage by modifying the tower design from a traditional mono-tower to a tripod. Due to a narrow stagnation zone the stress reversals and hence the damage accumulation in the blades is significantly smaller in the tripod tower configuration compared to the mono-tower. To make comparison meaningful simplified designs of the mono-tower and tripod tower are used, where the same amount of steel mass is used. Quantitative estimates of the effect of the tower shadow on the fatigue life of the blades in comparison to the damage contribution from turbulence and the influence of tower design was identified by the authors in a preliminary study Thoft-Christensen et al. [11]. Here, the expected value and standard

derivation of the fatigue life of the blades are estimated and compared for a turbine with a tripod tower and with a comparable standard mono-tower.

The blade stresses are calculated from a dynamic mechanical model based on a two degrees of freedom model. The displacements of the tower are neglected in the fatigue analysis of the blades. The self-induced aero-elastic loading and the turbulence loading are modeled by means of a quasi-static model linearized around the operational point, assuming that the time-scale for readjustment of the non-stationary flows during changes of the angle of attack is small compared to the fundamental eigen-vibration period of the blade. However, such memory effects are taken into consideration at the calculation of the aero-dynamic load during tower passage by the use of a rational approximation to the relevant indicial function. Furthermore, the rotational effect of the turbulence hitting the blade is taken into consideration.

The analysis is based on Monte Carlo simulation where 10 min realizations drawn from auto-spectral density of the rotational sampled turbulence process are generated, and the equations of motion and the differential equations for the blade and state variables of the rational memory filter are solved numerically. Next, the damage accumulation is calculated by rain-flow counting on the realizations of the bending stress.

Numerical examples demonstrated that the expected damage accumulation per unit of time in the turbine blades are reduced for the tripod when compared to the fatigue of the blade in a comparable mono-tower design. The variational coefficient of the fatigue life in the tower design is approximately of equal magnitude.

## 2. STRUCTURAL MODEL

The two tower configurations considered in this paper are defined in this section.

### 2.1. Definitions of tower configurations

The tubular mono-tower shown in Fig. 1 is designed with constant outer radius $R$ and varying thickness against bending moment $M$ determined from the rotor thrust $T$. The yaw axis is placed in the center $(R + e_0, 0)$ of the circular cross section. The constant distance from the yaw axis to the rotor plane is denoted $R_w$ defined as

$$R_w = R + e_0. \tag{1}$$

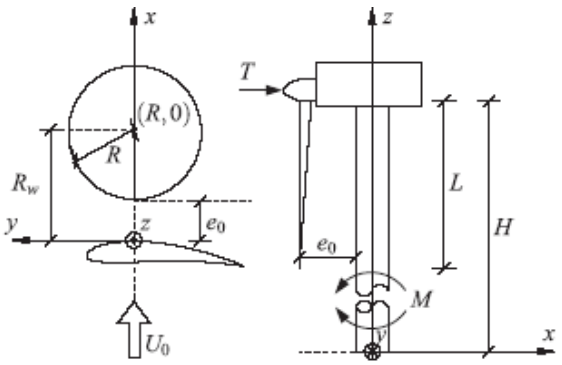


Fig. 1. Definition of coordinate systems, clearance and flow direction.

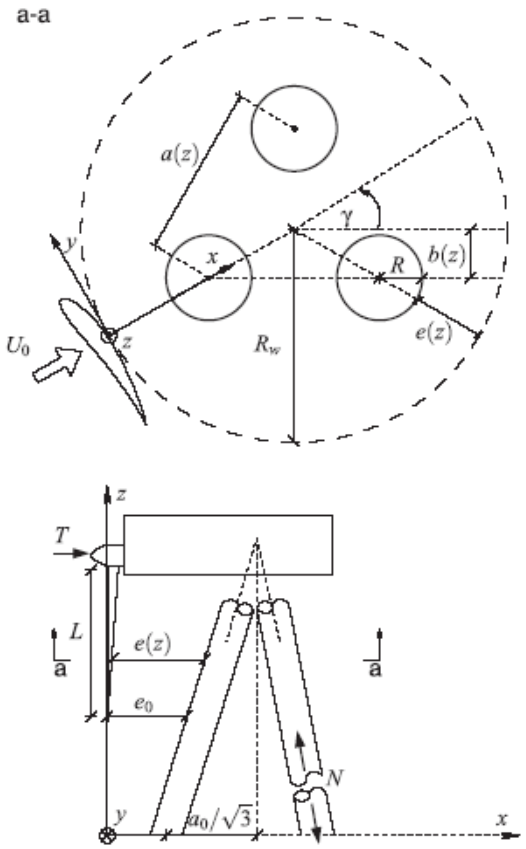


Fig. 2. Definition of coordinate system, clearance and flow direction. The yaw angle is $\gamma = \pi / 6$ in the elevation figure.

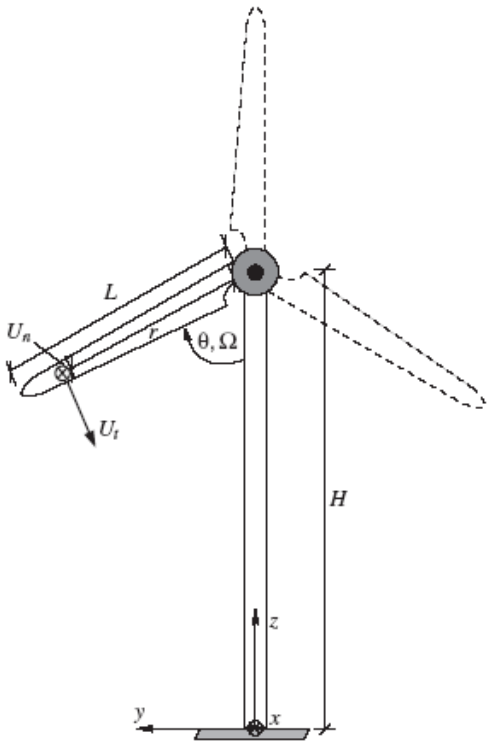


Fig. 3. Tower and rotating blade

The clearance $e_0$ is independent of the wind flow direction and the height of the tower i.e. the rotor is assumed to have zero tilt and coning, see Fig. 3. The tripod depicted in Fig. 2 is designed using the same total mass as for the mono-tower with the pods designed against buckling from axial force *N* and with the smallest possible outer radius R and constant thickness. The radii *R* of the individual towers are smaller compared to the standard mono-tower in Fig. 1.

The wind turbine is assumed to be yawed against the incoming mean wind U0, where the yaw angle is denoted c and positive in the z-direction, see Fig. 2. The yaw axis is placed in the center of gravity of the triangle formed by the tripod legs, see Fig. 2. The distance $a(z)$ between the center of the legs is dependent on the height z and the distance between the centers of the legs at the ground $a_0$

$$a(z) = a_0\left(1 - \frac{z}{H}\right) \tag{2}$$

where the height of the tower is *H*. The clearance $e_0$ is defined for a yaw angle $\gamma = \pi/6$ such that the rotor plane is able to pass the tripod legs. The clearance at the height z is given as

$$e(z) = e_0\frac{z}{H-L}, \tag{3}$$

Where $L$ is the length of the blade. The constant distance from the yaw axis to the rotor plane is defined for a yaw angle $\gamma = \pi/6$ and

$$R_w = R + e_0 + \frac{a(H-L)}{\sqrt{3}}, \tag{4}$$

which is the radius of the dashed circle in Fig. 2 and defines all possible positions of the rotor plane. Fig. 3 shows the geometry of a single blade of a horizontal axis upwind turbine, where $\Omega$ is the constant rotor speed. The position in the ($y$ - $z$) rotor plane of a cross section of the blade is defined in polar coordinates $(r,\theta)$. The corresponding Cartesian coordinates read

$$x = 0, \tag{5}$$

$$y = r\sin\theta, \tag{6}$$

$$z = H - r\cos\theta, \tag{7}$$

where $\theta$ is the azimuth angle, measured clockwise and zero when the blade is pointing downwards and *r* is the radius from the hub, see Fig. 3.

### 2.2 Wind velocity components

The wind velocity components upstream in the vicinity of the mono tower are determined from potential flow theory [12]

$$U_x = U_0\left(1 + R^2\frac{y^2 - (x-R-e_0)^2}{((x-R-e_0)^2 + y^2)^2}\right) \tag{8}$$

$$U_y = -2U_0R^2\frac{y(x-R-e_0)}{((x-R-e_0)^2 + y^2)^2}, \tag{9}$$

where ($R$ + $e_0$,0) is the coordinates of the cylinder center. Note that the solutions from the potential flow theories are only valid in front of the rotor plane in the up-wind

situations. In order to determine the potential flow around the two up-stream cylinders depicted in Fig. 2 an auxiliary (*x*',*y*')-coordinate system is introduced as shown in Fig. 4. The corresponding velocity $\left(U_{x'}(x',y'),U_{y'}(x',y')\right)$ components are determined by Alassar and El-Gebeily [19] in terms of a series solution for the stream function. A short outline of the resulting formulas has been given in the Appendix A.

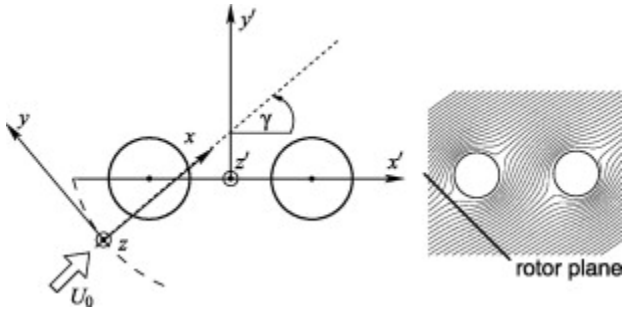


Fig. 4. Left: Definitions of coordinate systems (x, y) and (x′, y′) displaced with a distance b and rotated with the angle γ. Right: Plot of the stream function. The potential theory is only applicable in front of the rotor plane.

The corresponding components in the (*x*,y) coordinate system follows from the coordinate transformation

$$\begin{bmatrix} U_x(x,y) \\ U_y(x,y) \end{bmatrix} = \begin{bmatrix} \cos\gamma & \sin\gamma \\ -\sin\gamma & \cos\gamma \end{bmatrix} \begin{bmatrix} U_{x'}(x',y') \\ U_{y'}(x',y') \end{bmatrix}, \tag{10}$$

where the position coordinates in the two coordinate systems are related as

$$\begin{bmatrix} x' \\ y' \end{bmatrix} = \begin{bmatrix} \cos\gamma & -\sin\gamma \\ \sin\gamma & \cos\gamma \end{bmatrix} \begin{bmatrix} x \\ y \end{bmatrix} - \begin{bmatrix} R_w\cos\gamma \\ R_w\sin\gamma - b(z) \end{bmatrix}, \tag{11}$$

and the length $b(z)$ is given as, see Fig. 2

$$b(z) = a(z)\frac{\sqrt{3}}{6}. \tag{12}$$

The free mean wind speed $U_0$ at a height $z$ is found from

$$U_0 = u_{10}k_t \ln\left(\frac{z}{z_0}\right) \tag{13}$$

where $u_{10}$ is the 50-year return value of the 10-min mean wind speed at 10 m height and the terrain roughness parameters are $z_0$ = 0.03 and $k_t$ = 0.17. The wind velocity components depicted in Fig. 3 in the tangential and normal directions relative to the moving
blade read

$$U_n = U_x(1-a) \tag{14}$$
$$U_t = \Omega\, r(1+a'), \tag{15}$$

Where $\Omega$ is the rotational velocity of the blade, $r$ is the radial distance from hub to the cross section and $U_x$ is the velocity component upstream in the $x$-direction, respectively. The induction coefficients $a$ and $a_0$ are obtained from the Blade Element Momentum (BEM) theory, see Hansen [13], where the angle of attack $\alpha(r,t)$ is iterated from the velocity components. In the BEM iteration the instantaneous relative wind speed measured by an observer fixed to the cross section is $U = \sqrt{U_n^2 + U_t^2}$ and the

angle of attack is obtained from $\alpha = \varphi - \beta - \kappa$, where the angle $\varphi = \tan^{-1}(U_t / U_n)$, see Fig. 5, where $\kappa(r)$ is the pre-twist angle at the considered cross section and $\beta$ is the pitch angle of the blade.

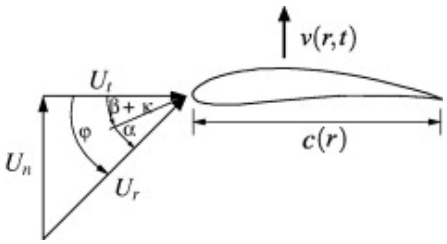


Fig. 5. Air-foil with chord length c and applied wind velocity components and the corresponding angles. The motion of the blade is denoted v(r, t) and depends on time t and the radius r measured from the hub to the specific air-foil.

### 2.3. Rotational turbulence spectrum

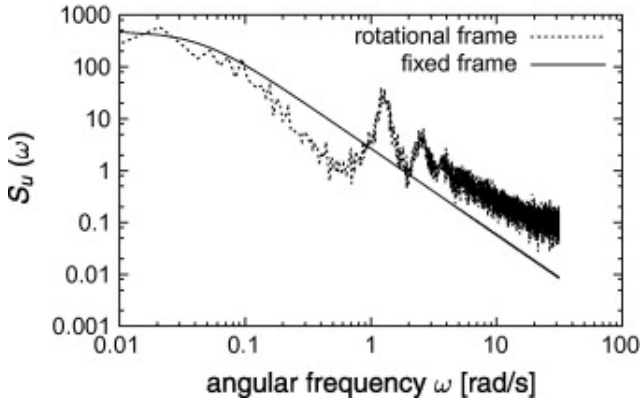


Fig. 6. One-sided auto-spectral density of wind turbulence for a fixed and rotating frame of reference.

The one-sided auto-spectral density function of the turbulence component *u* co-directional to the mean wind velocity $U_0$ is completely different, when measured in a fixed frame of reference and in a frame of reference fixed to a rotating blade as illustrated in Fig. 6. At large angular frequencies the spectrums approach asymptotically to a linear variation with the slope 5/3 in a double-logarithmic mapping in agreement with the Kolmogorov equilibrium theory for the inertial subrange. As seen the one-sided auto-spectral density measured in a rotating frame of reference shows marked peaks at the angular frequencies $\omega = \Omega$, $\omega = 2\Omega$, etc. The variance of the spectrum is identical to that of the spectrum in the fixed frame. Hence, the kinetic energy of the turbulence is conceived, but is considerably redistributed in the frequency space. The rotational effect is more pronounced at the tip of the wing and vanishes at the hub. Since the wind load is concentrated at the outer 1/3 of the blade, this effect is taken into consideration in the model of the blade. The turbulence model presented in [14] is here adopted to generate the turbulence wind fields with a turbulence intensity $I_v$ = 0.16 in Wind Turbine Class I [1]. A frozen turbulence box is generated for each mean wind speed considered in the fatigue analysis, which is convected into the rotor with the mean wind at hub in agreement with Taylor's hypothesis of frozen turbulence.

Next, the turbulence at a given cross section is obtained by interpolation among the grid points of the turbulence box.

### 2.4. Aero-dynamic model for tower shadow

The unsteady effects associated with a tower passage of the blades are important in the estimation of fatigue life. The physical significance behind the phenomena is studied in unsteady aero-dynamic experiments performed by Hand et al. [15], where data is available as validation to numerical models. Powles [10] presented wind speed measurements of the shadow wake behind a tubular steel tower. During tower passage the mean bending stresses are reduced because of the diminished thrust on the blade. Due to the aero-dynamic damping the dynamic amplification of the stress reversal is relatively small. This means that the shadow effect has minor influence on the extreme load case. The normal coefficient $c_N$ refers to the state where $\alpha$ is constant in time.

However, variations $d\alpha$ due to fluctuations of $U_n$ or $U_t$ is only observed in the normal coefficient after a transient period, where the flow conditions re-establish at a new stationary state. The fluctuations of $U_n$ during the tower passage has a resemblance to the vertical turbulence on an air-plane wing. Based on these observations Leisman [16] proposed an analog model for the time-delay effect on $c_N$ during a tower passage, where the present normal coefficient $\bar{c}_N = \bar{c}_N(t)$ is obtained from the convolution integral

$$\bar{c}_N(t) = 2\pi\left(\alpha(0)\psi(t) + \int_0^t \psi(t-\tau)d\alpha(\tau)\right), \tag{16}$$

of previous increments of the angle of attack, and where $\psi(t)$ is the Küssner function. By means of a rational approximation to this function the solution of the transient normal coefficient may be obtained from

$$\bar{c}_N(t) = 2\pi(A_1 c_1(t) + A_2 c_2(t)), \tag{17}$$

where $A_1 = 0.5$ and $A_2 = 0.5$ are non-dimensional coefficients. The coefficient $c_i$ ($i = 1, 2$) are obtained from the 1st order filter equations

$$\frac{\partial c_i}{\partial t} = \nu_i(\alpha(t) - c_i(t)), \tag{18}$$

where $\nu_i i = 1,2)$ are time scale factors defined as $\nu_1 = 0.26U_t/c$ and $\nu_2 = U_t/c$, see Fung [17].

### 2.5. Aero-elastic model for damping of the blades

The load increment $\Delta N$ of the normal load per unit length due to turbulence and the velocity $\dot{v}$ of the cross section is derived and added to the static load $N$. In case the load increment is in opposite direction to $\dot{v}$, energy is dissipated from the system,

which is denoted aero-elastic damping. Aero-elastic damping of the blades is an essential part of the structural behavior of the blades, which influences the fatigue life. An incompressible fluid is assumed and no memory effects are included in $\Delta N$, i.e. the load is imposed instantaneously as the angle of attack is changed. Lift $L$ and drag $D$ forces per unit length are computed from (see Fig. 7)

$$L(r,t) = \frac{1}{2}\rho U_r^2(r,t) C_L(r,\alpha) c(r), \tag{19}$$

$$D(r,t) = \frac{1}{2}\rho U_r^2(r,t) C_D(r,\alpha) c(r), \tag{20}$$

respectively, where the relative wind speed $U_r$ reads

$$U_r^2 = (U_0 + u - \dot{v})^2 + (\Omega r)^2, \tag{21}$$

which here includes the turbulence $u$ and velocity of the blade $\dot{v}$.

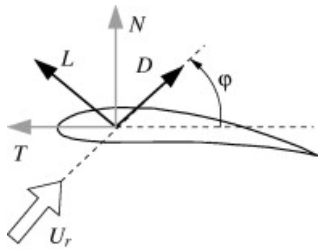


Fig. 7. Definition of lift ($L$), drag ($D$) forces and aero-dynamic loads ($T$; $N$) per unit length imposed to an air-foil.

The resulting so-called flow angle φ is accordingly defined as

$$\varphi = \tan\left(\frac{U_0 + u - \dot{v}}{\Omega r}\right)^{-1} \tag{22}$$

The turbulence and structural displacement of the blade changes the angle of attack and the angle φ, which consequently changes the load increment $\Delta N$ . Therefore, the angles are linearized around $u = \dot{v} = 0$ to determine the influence of the variations on the flow angle

$$\varphi = \varphi_0 + \Delta\varphi, \tag{23}$$

where the reference value $\varphi_0$ is

$$\varphi_0 = \tan\left(\frac{U_0}{\Omega r}\right)^{-1}, \tag{24}$$

and the increment $\Delta\varphi$ is found from linearization of (22)

$$\Delta\varphi = \Delta\alpha = \frac{1}{1 + \tan^2\varphi_0}\frac{u - \dot{v}}{\Omega r}. \tag{25}$$

Hence, the relative wind speed in (21) is approximated as

$$U_r^2 = U_{r,0}^2 + 2U_0(u - \dot{v}), \tag{26}$$

where the stationary wind speed is written as

$$U_{r,0}^2 = U_0^2 + (\Omega r)^2. \tag{27}$$

The lift load per unit length is written as

$$L = L_0 + \Delta L, \tag{28}$$

where $L_0$ refers to the reference angle of attack $\alpha_0$. The stationary wind speed $U_{r,0}$ is

$$L_0 = \frac{1}{2}\rho U_{r,0}^2 C_L(\alpha_0) c(r),$$

given as

(29)

where $\rho$ is the mass density of air, and $c(r)$ is the chord length. The increment $\Delta L$ is found from linearization of (19)

$$\Delta L = \frac{1}{2}\rho U_{r,0}^2 c(r)(u - \dot{v})\left(\frac{2U_0}{U_{r,0}^2}C_L(\alpha_0)\frac{1}{(1+\tan^2\varphi_0)\Omega r}\frac{\partial C_L(\alpha_0)}{\partial \alpha_0}\right). \tag{30}$$

Similarly, the drag coefficient is written as

$$D = D_0 + D\Delta, \tag{31}$$

with the stationary term

$$D_0 = \frac{1}{2}\rho U_{r,0}^2 C_D(\alpha_0)c(r), \tag{32}$$

and the quasi-static linearized increment given as

$$\Delta D = \frac{1}{2}\rho U_{r,0}^2 c(r)(u - \dot{v})\left(\frac{2U_0}{U_{r,0}^2}C_D(\alpha_0) + \frac{1}{(1+\tan^2\varphi_0)\Omega r}\frac{\partial C_D(\alpha_0)}{\partial \alpha_0}\right). \tag{33}$$

Finally, the normal load per unit length is found from

$$N = N_0 + \Delta N, \tag{34}$$

where $N_0$ is the static normal load per unit length given as

$$N_0(r, t+\Delta t) = \frac{1}{2}\rho U_r^2(r, t+\Delta t)\bar{c}_N(r, t+\Delta t)c(r), \tag{35}$$

with

$$c_N = c_L(r,\alpha)\cos\varphi_0 + c_D(r,\alpha)\sin\varphi_0. \tag{36}$$

The load increment $\Delta N$ is the quasi-static linearized increment

$$\Delta N = \Delta L\cos\varphi_0 + \Delta D\sin\varphi_0 - L_0\sin\varphi_0\Delta\varphi + D_0\cos\varphi_0\Delta\varphi, \tag{37}$$

where $\Delta\alpha$, $\Delta L$ and $\Delta D$ are given by (25), (33) and (30), respectively.

### 2.6. Mechanical model for the blade

The dynamic response of the blade during tower passage is primarily quasi-static and the dynamic effect is confined to the two lowest blade eigen modes. The dynamic component is relatively small when the boundary layer remains attached, where a substantial aero-dynamic damping is present. For this reason only these modes are included in the dynamic analysis. The blade characteristics are taken from a 5 MW NREL reference wind turbine; see Jonkman et al. [18], where the blade properties are discretized at 17 points along the blade. The blade characteristics can be found in Table 1. The two lowest eigen-modes are shown in Fig. 8 and the corresponding eigen-frequencies are listed in Table 2 together with the model characteristics adopted in the analysis. The displacement field $v(r, t)$ relative to the hub can be formulated as

$$v(r,t) = \sum_{i=1}^{2} \Phi_i(r)q_i(t), \tag{38}$$

where $\omega_i$ ($i$ = 1, 2) is the undamped angular flap-wise blade eigen-frequencies, and $\Phi_i$ is the related eigen-mode. $m_i$ and $F_i(t)$ denote the modal masses and the modal loads,

respectively, and can be computed from

$$m_i = \int_0^L \mu(x)\Phi_i(x)^2 dx, \tag{39}$$

$$F_i(t) = \int_0^L N(x,t)\Phi_i(x)dx. \tag{40}$$

The quadratures in (39) and (40) have been solved by Simpson integration. In what follows the convective velocity of the blade due to the vibration of the tower is ignored. Only the local velocity relative to the hub is considered. Therefore, the velocity and acceleration at a cross section can be computed from the derivatives of (38) as follows

$$\begin{aligned} \dot{v}(r,t) &\simeq \sum_{i=1}^{2} \Phi_i(r)\dot{q}_i(t), \\ \ddot{v}(r,t) &\simeq \sum_{i=1}^{2} \Phi_i(r)\ddot{q}_i(t). \end{aligned} \tag{41}$$

Finally, the modal coordinates for the two modes are given by the differential equation of motion

$$m_i\left(\ddot{q}_i + 2\zeta_i\omega_i\dot{q}_i + \omega_i^2 q_i\right) = F_i(t), \tag{42}$$

where $\zeta_i$ (i = 1, 2) are the modal damping ratios including due to structural. In the analysis aero-dynamic damping is only included in the first eigen-mode. Applying D'Alembert's principle the bending moment in the blade becomes

$$M(r,t) = \int_r^L (x-r)(N(x,t) - \mu(x)\,\ddot{v}(x,t))dx. \tag{43}$$

| Section | Air-foil | Radius r (m) | Chord c (m) | EI $10^6$ (Nm) | μ (kg/m) | κ (deg) |
|---|---|---|---|---|---|---|
| 1 | Cylinder | 2.8667 | 3.542 | 19497.80 | 740.550 | 13.308 |
| 2 | Cylinder | 5.6000 | 3.854 | 10220.60 | 450.275 | 13.308 |
| 3 | Cylinder | 8.3333 | 4.167 | 6884.44 | 382.062 | 13.308 |
| 4 | DU40A17 | 11.7500 | 4.557 | 7271.66 | 416.820 | 13.181 |
| 5 | DU35A17 | 15.8500 | 4.652 | 4948.49 | 349.477 | 11.072 |
| 6 | DU35A17 | 19.9500 | 4.458 | 4501.40 | 339.333 | 10.232 |
| 7 | DU30A17 | 24.0500 | 4.249 | 3995.28 | 321.990 | 9.110 |
| 8 | DU25A17 | 28.1500 | 4.007 | 3447.14 | 294.734 | 7.932 |
| 9 | DU25A17 | 32.2500 | 3.748 | 2734.24 | 263.343 | 6.711 |
| 10 | DU21A17 | 36.3500 | 3.502 | 2334.03 | 241.666 | 5.546 |
| 11 | DU21A17 | 40.4500 | 3.256 | 1584.10 | 200.293 | 4.401 |
| 12 | NACA64A17 | 44.5500 | 3.010 | 1183.68 | 165.094 | 3.332 |
| 13 | NACA64A17 | 48.6500 | 2.764 | 797.81 | 138.935 | 2.503 |
| 14 | NACA64A17 | 52.7500 | 2.518 | 518.19 | 107.264 | 1.730 |
| 15 | NACA64A17 | 56.1667 | 2.313 | 395.12 | 98.776 | 1.342 |
| 16 | NACA64A17 | 58.9000 | 2.086 | 304.73 | 72.906 | 0.574 |
| 17 | NACA64A17 | 61.6333 | 1.419 | 158.81 | 59.340 | 0.253 |

Table 1. Seventeen sections along the blade with a distance r measured from the hub with the air-foils names, chord lengths c, bending stiffness EI, mass per unit length μ and pre-twist κ, respectively.

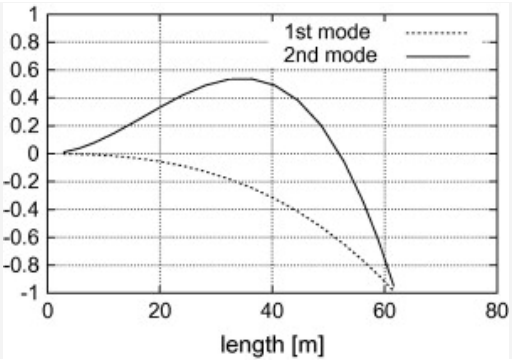


Figure 8. 1st and 2nd blade eigen-modes.

| | | | |
|---|---|---|---|
| Eigen-frequency | $\omega_1$, $\omega_2$ | 6.32, 30.54 | rad/s |
| Hub height | $H$ | 90 | m |
| Mono tower radius | $R$ | 3.0 | m |
| Tripod radii | $R$ | 1.0 | m |
| Tubular thickness (mono) | $t$ | 0.09 | m |
| Tubular thickness (tripod) | $t$ | 0.03 | m |
| Total amount of steel (both) | | 25.5 | $m^3$ |
| Blade length | $L$ | 62 | m |
| Hub diameter of blade | $D$ | 3.8 | m |
| Clearance | $e_0$ | 4.0 | m |
| Leg distance (tripod) | $a_0$ | 8.0 | m |
| Rotational speed | $\Omega$ | 1.26 | rad/s |
| Life time | | 30 | year |
| Number of samples | $Nc$ | 20 | |
| Sampling time | T | 600 | s |
| Young's modulus of blade | $E$ | $0.05\ 10^{12}$ | $N/m^2$ |
| Damping ratios | $\zeta_1$, $\zeta_2$ | 0.01; 0.01 | |
| Cut-in; cut-out wind velocity | $u^{in}$, $u^{out}$ | 5;25 | m/s |
| Yaw angle interval | $T$ | $[-\pi/2\ ,\ \pi/2]$ | rad |

Table 2. Model characteristics.

### 2.7. Estimation of fatigue life

Fatigue properties of fiberglass composite materials are discussed by Sutherland and Mandell [22], where an optimal constant life diagram is proposed. In Toft and Sørensen [23] the constant life diagram is further developed, where experimental results are

adopted. The fatigue data used for the fiber material of the blade is taken from [23] and reported in constant life diagram in Fig. 9. The procedure in the IEC norm [1] is followed to compute the fatigue life of a wind turbine blade. In composite materials not only the stress amplitude but also the mean stress is important for the fatigue life. The stress points are evaluated using the constant life diagram in Fig. 9. The $R_f$ values define the ratio between the maximum and minimum stress in a stress cycle i.e. $R_f = -1$ means that the maximum tensile stress equals the minimum compressive stress. The mean wind velocity $U_{10}$ at 10 m altitude and the yaw angle $\Gamma$ are assumed to be independent random variables. $U_{10}$ is Rayleigh distributed

$$p_{U_{10}}(u_{10}) = \frac{u_{10}\pi}{2V_{\text{avg}}} \exp\left(-\pi\left(\frac{u_{10}}{2V_{\text{avg}}}\right)^2\right), \tag{44}$$

where the average wind velocity is $V_{\text{avg}} = 0.2V_{\text{ref}}$ with the reference velocity defined as $V_{\text{ref}} = 50$ m/s in Wind Turbine Class I [1]. The yaw angle is assumed to be uniformly distributed in the interval $[-\pi/2, \pi/2]$ rad.

$$p_{\Gamma}(\gamma) = \frac{1}{\pi}. \tag{45}$$

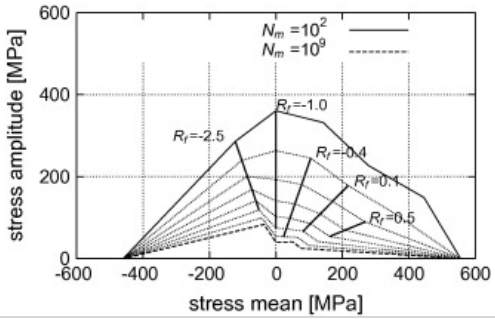


Fig. 9. Constant life diagram, where $N = 10^2$ and $N = 10^9$ indicate the lower and upper bound for the number of cycles.

For a specific yaw angle and mean wind velocity the damage state is computed from Miners sum according to

$$D(\gamma, u_{10}) = \frac{\text{Lifetime}}{T} \int_0^{\infty} \frac{n_{st}}{N_m} d\sigma, \tag{46}$$

where $n_{\text{st}}$ is the number of cycles in the referential time interval $T$ with a specific stress amplitude and mean stress using a Rain Flow Counting algorithm. The maximum number of cycles, characteristic for the material exposed to a constant stress range and mean stress, is denoted $N_m$ in Eq. (46), and is determined from the constant life diagram in Fig. 9. The damage is a random variable due to the turbulence field. Totally, $N_c$ samples of $D(\gamma, u_{10})$ is performed in the Monte Carlo simulation. The conditional mean damage value is estimated from

$$\mu(\gamma, u_{10}) = \frac{1}{N_c} \sum_{i=1}^{N_c} d_i(\gamma, u_{10}), \tag{47}$$

whereas the corresponding damage standard derivation reads

$$\sigma(\gamma, u_{10}) = \frac{1}{N_c} \sum_{j=1}^{N_c} (d_i(\gamma, u_{10}) - \mu(\gamma, u_{10}))^2. \tag{48}$$

Finally, the unconditional mean damage value $\mu_D$ and standard derivation $\sigma_D$ during the life time of the wind turbine are computed from

$$\mu_D = \int_{u^{in}}^{u^{out}} \int_{-\pi/2}^{\pi/2} \mu(\gamma, u_{10}) p_{U_{10}}(u_{10}) p_\Gamma(\gamma) d\gamma du_{10}, \tag{49}$$

$$\sigma_D = \int_{u^{in}}^{u^{out}} \int_{-\pi/2}^{\pi/2} \sigma(\gamma, u_{10}) p_{U_{10}}(u_{10}) p_\Gamma(\gamma) d\gamma du_{10}, \tag{50}$$

where $u_{10}^{in}$ and $u_{10}^{out}$ is the cut-in and cut-out operational wind velocities, respectively.

## 3. Numerical example

The fatigue damage of a wind turbine blade is estimated when the wind turbine blade is attached to a mono-and tripod tower. The thickness and radii are adjusted so that the amount of steel used in the mono-and tripod configuration is identical. In this example the distance between the tripod legs at $z = 0$ m is $a_0 = 8$ m and the radii of the cylinders are $R = 1$ m with a thickness $t = 0.03$ m. The radius of the mono tower is 3 m with a thickness $t = 0.09$ m. The radii and thickness are assumed to be independent of the height. The mean wind is computed from Eq. (13). The air-foil characteristics at specific cross-sections are presented in Table 1 and taken from a 5 MW NREL reference wind turbine; see Jonkman et al. [18]. The drag and lift coefficients and the derivatives for an air-foil DU30A17 are presented in Fig. 10 and Fig. 11, respectively.

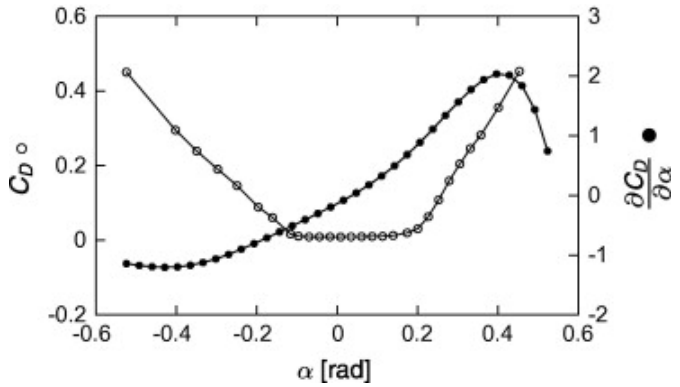


Fig. 10. The drag coefficient *CD* and the derivative dependent on the angle of attack $\alpha$ for an air-foil DU30A17.

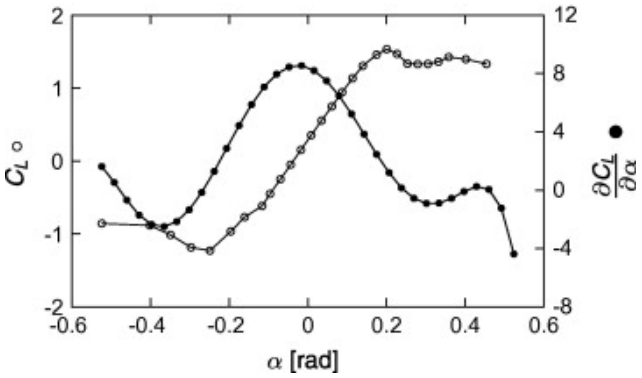


Fig. 11. The lift coefficient *CL* and the derivative dependent on the angle of attack $\alpha$ for an air-foil DU30A17.

The derivatives are found from the derivatives of the polynomial fits to the lift and drag coefficients dependent on the angle of attack $\alpha$. A characteristic moment variation dependent on azimuth angle $\Theta$ and yaw angle $\gamma$ is presented in Fig. 12, where the mono and tripod towers are compared when the turbulence component and the inertia term in Eq. (43) are not included. When the yaw angle $\gamma = 0$ the rotor plane is closest to one tripod leg with radius $R = 1$ m. In this situation, the results can be compared to the blade passage of a mono tower with radius $R = 4$ m, see Fig. 12a.

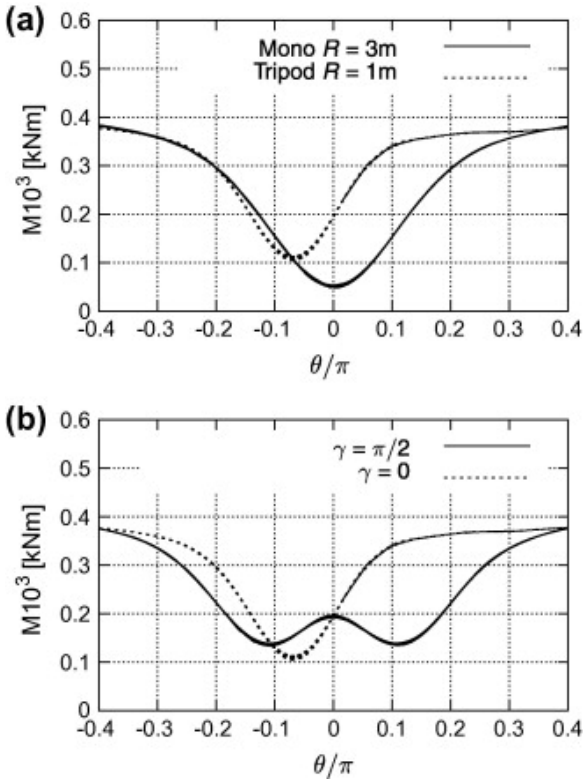


Fig. 12. Bending moment M in the blade hub as a function of the azimuth angle θ where (a) compares the blade passage of a mono tower and the tripod tower ($\gamma = 0$) and (b) compares the blade passage in the tripod for two different yaw angles.

The blade experiences a wider shadow zone when the radius is increased and consequently the moment shows a larger variation. In Fig. 12b, the variation of the bending moment dependent on the azimuth angle and yaw angle is presented. For a yaw angle $\gamma = \pi/2$ the blade passes two towers with radius $R = 1$ m with equal clearance Thus, the blades experience two stagnation zones. The moment variation is symmetric with respect to the azimuth angle and the moment variation is lower.

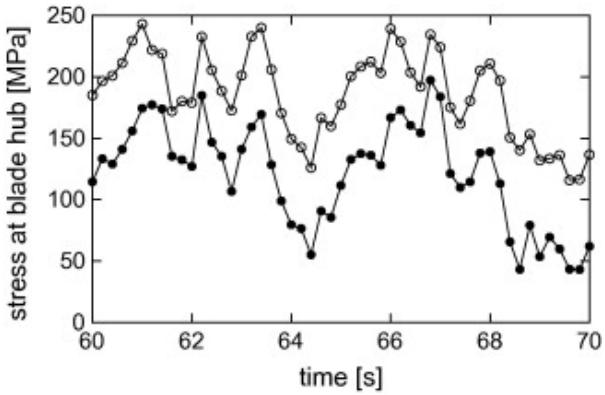


Fig. 13. Normal stress in the blade hub as a function of the azimuth angle θ with $u_{10} = 15$ m/s and $\gamma = 0$ rad. ∘: mono tower and •: tripod tower.

Fig. 13 presents the variation of the normal stress in the hub of the blade, when the blade passes a mono tower and tripod tower in case of a yaw angle $\gamma = 0$ deg and free wind velocity $u_{10} = 15$ m/s. The Miner sum linked to $\gamma = 0$ rad and $u_{10} = 15$ m/s is presented in Fig. 14, where each sample corresponds to a random turbulence field. This result indicates that the fatigue damage is lower when the tripod tower is used, where the shadow zones are small compared to the case with a standard mono tower. Table 3 shows the results from a complete analysis, where all yaw angles and mean wind velocities are included for both the tripod and mono tower. The final unconditional mean damage value $\mu_D$ and standard derivation $\sigma_D$ is presented in Table 3. The damage state is lower for the tripod configuration. Therefore, with the adopted assumptions and simplifications the lifetime is increased for a tripod configuration.

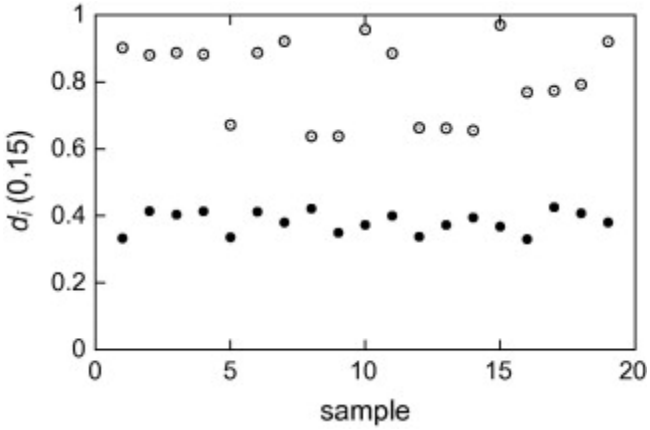


Fig. 14. Samples of Miners sum, Eq. (46), in case of a mean wind u10 = 15 m/s and yaw angle γ = 0 rad. ∘: mono tower and •: tripod tower.

| | Mono tower | Tripod tower |
|---|---|---|
| $\mu_D$ | 0.532 | 0.324 |
| $\sigma_D$ | 0.078 | 0.042 |

Table 3. Unconditional mean damage $\mu_D$ and standard derivation $\sigma_D$ in case of a mono tower and tripod configuration.

## 4. Conclusions

A computational framework for the analysis of fatigue life in wind turbine blades due to shadow effects is presented. A tripod configuration is proposed to replace the standard mono tower. In this way the shadow zones are decreased because the tripod tubular legs have a small radius compared to the radius of the mono tower. Although, the wind turbine blade experiences more disturbances because of the three tripod legs, the total fatigue damage is decreased. The framework consists of an unsteady aero-dynamic model representing the delay when the blade passes the shadow zone. An aero-elastic model is implemented to account for the damping related to interaction between load and the mechanical response. The mechanical model for the wind turbine blade is based on the two lowest eigen-modes. The wind velocity components are found from potential theory, where the interaction between the cylinders is taken into account. A turbulence field is included from a rotational turbulence spectrum model. The final mean damage and standard derivation are estimated, where the turbulence is the stochastic variable.

The results indicate that the fatigue damage is significantly lower when the wind turbine blade is attached to a tripod configuration. Note this is a relative comparison of the two tower configurations. A different composite material changes the constant life diagram. However, the relative fatigue life of the two systems is unchanged. The practical aspects concerning the construction and implementation of the tripod solution is not considered.

## Acknowledgments

S.R.K. Nielsen acknowledges the support of Danish Energy Authority under the Grant No. EFPO7-II: “Estimation of Extreme Responses and Failure Probabilities of Wind Turbines under Normal Operations by means of Controlled Monte Carlo Simulations”.

## Appendix A. Potential flow around two aligned cylinders

The wind velocity components related to an arbitrarily oriented flow passing two aligned cylinders are determined from the work by Alassar [19], where a closed form solution is presented. The theoretical findings are verified and compared to numerical solutions in [21]. The stream functions related to the potential flow read

$$\psi = 2bU_0\left(\psi_x \cos\gamma + \psi_y \sin\gamma\right), \tag{51}$$

$$\begin{aligned}\psi_x = &-\frac{\sinh(\xi)}{2(\cosh\xi-\cos\eta)} + \sum_{n=1}^{\infty}\frac{\cos(n\eta)\exp(-n\xi_2)\sinh n(\xi-\xi_1)}{\sinh n(\xi_2-\xi_1)} \\ &+ \sum_{n=1}^{\infty}\frac{\cos(n\eta)\exp(+n\xi_1)\sinh n(\xi-\xi_2)}{\sinh n(\xi_2-\xi_1)} + \sum_{n=1}^{\infty}\frac{\sinh n(\xi_2+\xi_1)}{\sinh n(\xi_2-\xi_1)},\end{aligned} \tag{52}$$

$$\psi_y = \frac{\sin(\eta)}{2(\cosh\xi - \cos\eta)} - \sum_{n=1}^{\infty} \frac{\sin(n\eta)\exp(-n\xi_2)\sinh n(\xi - \xi_1)}{\sinh n(\xi_2 - \xi_1)} + \sum_{n=1}^{\infty} \frac{\sin(n\eta)\exp(+n\xi_1)\sinh n(\xi - \xi_2)}{\sinh n(\xi_2 - \xi_1)}, \tag{53}$$

where indices $x$ and $y$ indicate flow perpendicular and parallel to the tripod legs, respectively. The stream functions are expressed in bipolar coordinates ($\xi$ , $\eta$ ). In Eq. (51), $U_0$ is the free mean wind speed orientated with an angle $\gamma$ with respect to the two cylinders, see Fig. 4. In the following equations the radii of the cylinders are identical.

The distance $b$ is defined as

$$b = R\sinh(\xi_2) \tag{54}$$

where $a(z)$ is the physical distance between two tripod legs. The coordinate $\xi_2$ express the center of the second cylinder and is determined from

$$\xi_2 = \operatorname{arccosh}\frac{a(z)}{2R}, \tag{55}$$

and $\xi_1 = -\xi 2$ is the coordinate to the first cylinder. The relation between the bipolar and Cartesian coordinates is defined [20] as

$$x = \frac{b\sinh\xi}{\cosh\xi - \cos\eta} \quad y = \frac{b\sin\eta}{\cosh\xi - \cos\eta}, \tag{56}$$

and after mathematically manipulations the inverse relations can be derived as

$$\xi = \operatorname{arccoth}\left(\frac{b^2 + x^2 + y^2}{2bx}\right), \tag{57}$$

and

$$\eta = \operatorname{arccot}\left(\frac{-b^2 + x^2 + y^2}{2by}\right). \tag{58}$$

The wind velocity components ($U_x$,$U_y$) can be determined from

$$\begin{Bmatrix} U_{x'} \\ U_{y'} \end{Bmatrix} = \begin{bmatrix} \frac{\partial x}{\partial \xi} & \frac{\partial y}{\partial \xi} \\ \frac{\partial x}{\partial \eta} & \frac{\partial x}{\partial \eta} \end{bmatrix}^{-1} \begin{Bmatrix} \frac{\partial \psi}{\partial \xi} \\ \frac{\partial \psi}{\partial \eta} \end{Bmatrix}, \tag{59}$$

where $U_{x'} = \frac{\partial \psi}{\partial y}$ and $U_{y'} = -\frac{\partial \psi}{\partial x}$.

These velocity components need to be transformed back into the (x, y) coordinated system.

## References

[1] IEC. Wind turbine-part 1 design requirement. IEC 61400-1:2005(E) 3rd ed.

[2] T. Wang, F.N. Coton. A high resolution tower shadow model for downwind turbines. J. Wind Eng Ind Aerodyn, 89 (2001), pp. 873–892.

[3] D.S.L. Dolan, P.W. Lehn. Simulation model of wind turbine 3p torque oscillations due to wind shear and tower shadow. IEEE Trans Energy Convers, 21 (2006), pp. 717–724

[4] X. Munduate, F.N. Coton, R.A.M. Galbraith. An investigation of the aerodynamic

response of a wind turbine blade to tower shadow. J. Sol Energy Eng, 126 (2004), pp. 1034–1040.
[5] Munduate X, Coton FN. Identification of dynamic stall regions on horizontal axis wind turbines. In: 19th ASME wind energy symposium, Reno 2000; Paper:2000-0039.
[6] Wang T. An examination of two tower-shadow modelling strategies for downwind wind turbines. In: AIAA, aerospace sciences meeting and exhibit, 36th, and 1998 ASME wind energy symposium, Reno, NV, January 12–15, 1998, Collection of Technical Papers (A98-16844 03-44), Reston, VA/New York, American Institute of Aeronautics and Astronautics, Inc./A; 1998.
[7] Rosas PAC, Sørensen P, Binder H. Fast wind modelling for wind turbines. In: Proceedings (on CD-ROM), Wind power for the 21 century: EUWEC special topic conference and exhibition 2527, September 2000. p. 184–7.
[8] Crawford CA. Advanced engineering models for wind turbines with application to the design of a coning rotor concept. Dissertation, Trinity College Department of Engineering, University of Cambridge; 2006.
[9] Moriarty PJ, Hansen AC. AeroDyn Theory Manual. National Renewable Energy Laboratory United States. NREL/TP; 2005.
[10] S.R.J. Powles. The effects of tower shadow on the dynamics of a horizontal-axis wind turbine. Wind Eng, 7 (1983), pp. 26–42.
[11] Thoft-Christensen P, Pedersen RR, Nielsen SRK. Numerical estimation of fatigue life of wind turbines due to shadow effect. In: Proceedings of the 10th international conference on structural safety and reliability, Kansai University Japan; 2009.
[12] L.M. Milne-Thompson.Theoretical aerodynamics. Dover Publications (1996)
[13] M.O.L. Hansen. Aerodynamics of wind turbines. James & James (2001)
[14] Gilling L, Nielsen SRK, Sørensen NN. Generation of synthetic turbulence in arbitrary domains. In: Proceedings of the 10th international conference on structural safety and reliability, Kansai University Japan; 2009.
[15] Hand MM, Simms DA, Fingersh LJ, Jager DW, Cotrell JR, Shreck SJ, et al. Unsteady aerodynamics experiment phase VI: wind tunnel test configurations and available data campaigns. National Renewable Laboratory United States. NREL/TP-500-29955; 2001.
[16] Leishman JG. Challenges in modelling the unsteady aerodynamics of wind turbines. In: 21st ASME wind energy symposium Reno, United States; 2001.
[17] Y.C. Fung. An introduction to the theory of aeroelasticity. Dover Publications (2002).
[18] Jonkman J, Butterfield SS, Musial W, Scott G. Definition of a 5-mw reference wind turbine for offshore system development. NREL/TP-500-38060, Golden, National Renewable Energy Laboratory, in press.
[19] R.S. Alassar, M.A. El-Gebeily. Inviscid flow past two cylinders. J. Fluids Eng, 131 (2009), pp. 0545011–0545016.
[20] R.A. Ibrahim. Liquid sloshing dynamics: theory and applications. University Print Cambridge (2002)
[21] Pedersen RR, Leth S. Proceedings of the 22nd Nordic seminar on computational mechanics, NSCM, Aalborg University Denmark; 2009.
[22] H.J. Sutherland, J.F. Mandell. Optimized constant-life diagram for the analysis of fiberglass composites used in wind turbine blades. J. Sol Energy Eng-Trans ASME, 127 (2005), pp. 563–569

[23] Toft H.S, Sørensen J.D. Stochastic models for strength of wind turbine blades using tests. In: Proceedings of EWEC, Europe's premier wind energy event, Brussels Belgium; 2008.